nature nanotechnology

ARTICLES

PUBLISHED ONLINE: 26 OCTOBER 2015 | DOI: 10.1038/NNANO.2015.243

Macromolecular crowding creates heterogeneous environments of gene expression in picolitre droplets

Maike M. K. Hansen[1], Lenny H. H. Meijer[2], Evan Spruijt[3], Roel J. M. Maas[1], Marta Ventosa Rosquelles[1], Joost Groen[1], Hans A. Heus[1] and Wilhelm T. S. Huck[1]*

Understanding the dynamics of complex enzymatic reactions in highly crowded small volumes is crucial for the development of synthetic minimal cells. Compartmentalized biochemical reactions in cell-sized containers exhibit a degree of randomness due to the small number of molecules involved. However, it is unknown how the physical environment contributes to the stochastic nature of multistep enzymatic processes. Here, we present a robust method to quantify gene expression noise *in vitro* using droplet microfluidics. We study the changes in stochasticity in the cell-free gene expression of two genes compartmentalized within droplets as a function of DNA copy number and macromolecular crowding. We find that decreased diffusion caused by a crowded environment leads to the spontaneous formation of heterogeneous microenvironments of mRNA as local production rates exceed the diffusion rates of macromolecules. This heterogeneity leads to a higher probability of the molecular machinery staying in the same microenvironment, directly increasing the system's stochasticity.

Noise is present in all living cells. It has been studied in prokaryotes and eukaryotes[1], as well as stem[2,3] and cancer cells[4], and cells expressing viruses[5]. Gene expression is a key example of a complex stochastic enzymatic process. Careful analysis of variations in mRNA and protein levels has revealed the importance of both the amplitude and typical decay time of noise and the ability of cells to exploit or suppress noise in gene expression[6–9]. Unlike deterministic models of gene expression, which are used to predict dynamics over large populations, stochastic models can correctly predict the dynamics of gene expression at the single cell level[10]. Recently, it has become apparent that the stochastic nature of many biochemical processes cannot be ignored *in vivo* and *in vitro*. The two-reporter system developed by Elowitz and colleagues[11] as a reliable method to estimate[12] the magnitude of variation in gene expression has been used to study noise both *in vivo* and *in vitro*[12–14]. Because reaction networks inside the cell involve numerous components, each at a very low concentration, an important degree of randomness is expected[15–18]. It is generally accepted that this stochasticity is due to both the low concentrations of reacting molecules and the random nature of molecular collisions due to diffusion. However, this inherent stochastic nature of chemical reactions is typically ignored when studying chemical reactions in dilute, well-stirred reactors. In contrast, the cell's interior is an inhomogeneous, crowded environment. In bacteria, for example, ~30% of the cell volume is occupied by macromolecules, resulting in highly reduced diffusion[19,20]. Such a crowded environment can lead to spontaneous spatial organization due to the severely limited diffusion of mRNA molecules[21]. Moreover, macromolecular crowding affects the dynamics and thus reaction rates of cellular processes[22]. Further studies have shown that prokaryotic cells are less fluid-like than originally anticipated and can exhibit dynamical heterogeneity and glassy features[23,24]. Most studies thus far have dealt with either the quantification of noise[25], or how cells exploit or suppress noise[1,26]. It has previously been shown *in silico*[27] that diffusivity plays a role in gene expression noise, but no experimental work has estimated the magnitude of the effect of cellular composition or crowded environment within a cell-sized compartment on the stochasticity of biochemical reactions.

To quantify the various contributions to noise in *in vitro* gene expression, we have studied the transcription and translation of cyan fluorescent protein (CFP) and yellow fluorescent protein (YFP) in picolitre droplets[14,28,29]. Picolitre droplets are ideally suited for the study of biochemical reactions involving very small numbers of reactants[30,31]. The microfluidic approach allows for precise control over droplet volume, producing a large number of monodisperse water-in-oil droplets at rates up to 500 droplets per second (Supplementary Fig. 1). The large number of identical droplets provides high reproducibility. We can therefore measure stochasticity in gene expression as a function of DNA copy number and macromolecular crowding. Our results emphasize the complex interplay between the cellular environment and the dynamics of cellular processes.

Effect of copy number on uncorrelated noise

One typically distinguishes two types of noise: extrinsic and intrinsic[11]. When comparing the expression of two identical yet independent genes *in vivo*, fluctuations in the amounts or states of cellular material lead to correlated fluctuations in the expression of both proteins, and this is considered extrinsic noise. On the other hand, the stochasticity of a biochemical process or other factors leading to uncorrelated fluctuations in the numbers of either protein is considered intrinsic noise. In line with these explanations, but to avoid confusion with other *in vivo* experiments and taking into account our experimental set-up, we make the distinction between uncorrelated and correlated noise (Fig. 1a,b)[8,32,33]. Correlated noise arises from the inhomogeneous Poisson

[1]Radboud University, Institute for Molecules and Materials, Heyendaalseweg 135, 6525 AJ Nijmegen, The Netherlands. [2]Eindhoven University of Technology, Institute for Complex Molecular Systems and Computational Biology Group, Eindhoven 5600 MB, The Netherlands. [3]ESPCI ParisTech, Laboratoire de Physique et Mécanique des Milieux Hétérogènes, UMR 7636 du CNRS, Paris 75005, France. *e-mail: w.huck@science.ru.nl

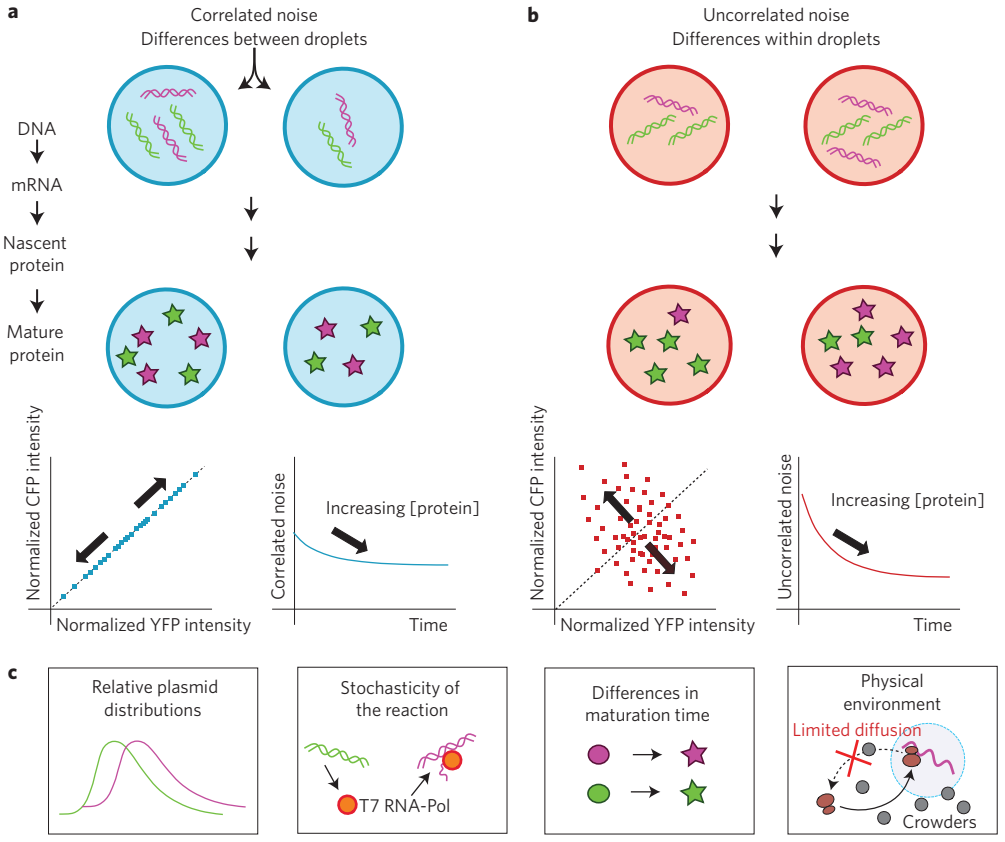

Figure 1 | Correlated versus uncorrelated noise. a, Correlated noise is dominated by the Poisson distribution of reactants over the population of droplets, causing differences in the CFP and YFP levels between droplets; that is, the CFP and YFP levels within a droplet are correlated. **b**, Uncorrelated noise is the noise orthogonal to the line CFP = YFP. **c**, Uncorrelated noise is caused by relative differences in the Poisson distributions of plasmids, the stochasticity of the biochemical reactions, differences in the maturation times of CFP and YFP, and the effect of a crowded environment with limited diffusion.

distribution of molecules among different bioreactors, leading to droplet-to-droplet variation in expression, but within one bioreactor CFP and YFP levels are correlated. Correlated noise can be calculated from the covariance between normalized CFP (I_{CFP}) and YFP (I_{YFP}) intensities over all droplets. Uncorrelated noise can be seen as the extent to which the output of two reactions in the same confined space differs[25], and is calculated as the normalized root-mean-square distance from the line CFP = YFP. Various physical and biochemical factors contribute to the uncorrelated noise in our experiments (Fig. 1c). First, as a result of our experimental design using plasmids, our uncorrelated noise is influenced by differences in the relative Poisson distributions of the CFP and YFP plasmids. This contribution is not present in the original approach taken by Elowitz and co-workers, and the uncorrelated noise we discuss here should therefore not be confused with their intrinsic noise[11]. Second, uncorrelated noise arises from the randomness inherent to biochemical reactions and increases with decreasing numbers of reacting molecules. Third, there is a possible contribution from differences in the maturation times of CFP and YFP. Finally, as we demonstrate in this Article, the physical environment within one droplet, reflected for instance by limited diffusion or crowding, can lead to an enhancement of the variations in the reaction rates, and makes an additional contribution to uncorrelated noise.

By measuring the fluorescence intensity of YFP (pRSET-YFP) and CFP (pRSET-CFP) (Supplementary Fig. 2) for a population of 300 droplets every 10 min (Fig. 2a, Supplementary Fig. 3) and thus following the expression of both proteins per droplet, we can calculate the time evolution of uncorrelated, correlated and total noise in our system (Fig. 2b.). There is a constant increase in protein concentrations because there is no observable protein degradation (Supplementary Fig. 4). Figure 2b shows that the noise levels decrease over time, which is in agreement with the observed increase in protein concentration over time (see Supplementary Fig. 5 for all expression and noise curves). We first varied the DNA concentration from 16,000 copies to 100 copies per droplet for both the CFP and YFP plasmids, and the concentrations of all other components were kept constant throughout the experiments. Plotting the normalized fluorescence intensities of CFP and YFP in each droplet with either high (16,000) or low (190) plasmid copy numbers 100 min after the start of fluorescence increase (Fig. 2c), we can clearly observe a significant increase in uncorrelated noise (the spread of data points orthogonal to the axis CFP = YFP) as the copy number decreases. These experiments were repeated for a wide range of initial plasmid concentrations. The correlated noise, that is, the distribution of components over the droplets (Fig. 2d, blue open circles), shows no statistically significant correlation (Spearman's rho correlation of −0.393) with plasmid concentration. Uncorrelated noise, however, shows a clear negative correlation (−0.929, significant at the 0.01 level) with plasmid concentration (Fig. 2d, red filled squares), which can be due to the gene expression becoming increasingly stochastic with a lower numbers of molecules involved. This is in line with the theory of stochasticity, which states that the relative importance of the fluctuations involved increases as the reactant number decreases[15]. This trend is also visible 10, 30 and 50 min after the start of expression (Fig. 2e and Supplementary Fig. 7), indicating that it is independent of the moment the image was taken. We chose to calculate the noise

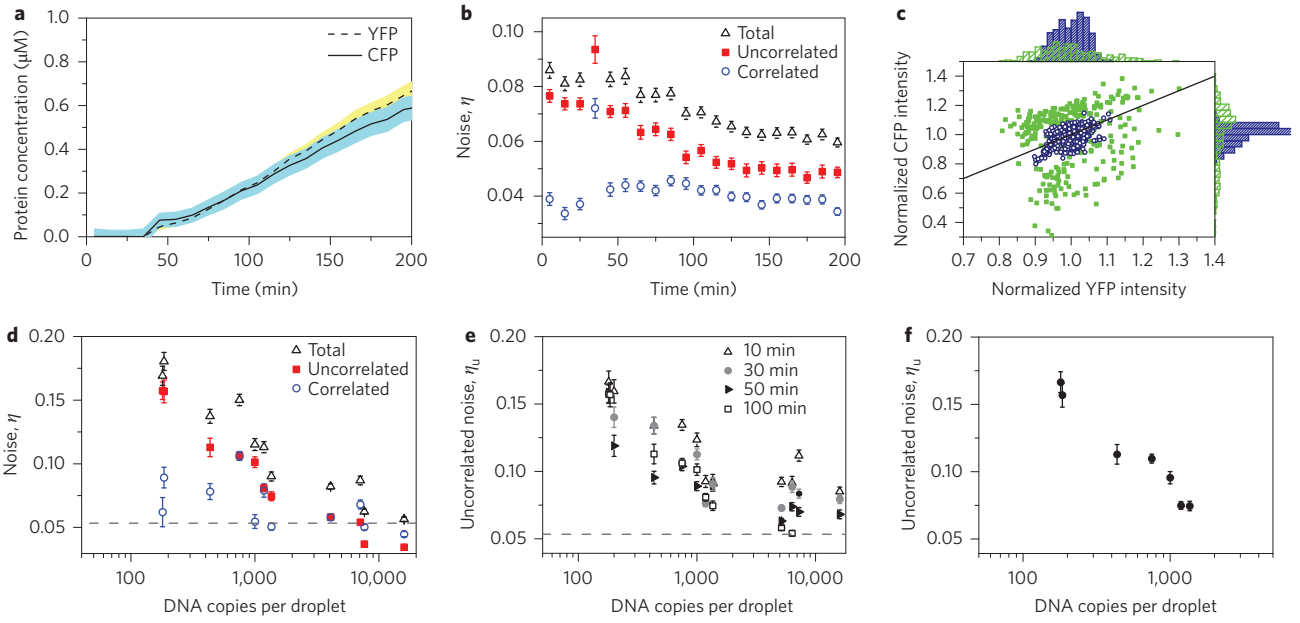

Figure 2 | Effect of decreased copy number on inherent stochasticity of gene expression in pico-reactors. a, Average CFP and YFP expression over all droplets. **b**, Uncorrelated, correlated and total noise values over time for 7,600 copies of each plasmid per droplet. **c**, Normalized CFP versus normalized YFP intensities of the whole population of droplets at 100 min after the start of fluorescence increase for 190 (green filled squares) and 16,000 (blue open circles) copies of each plasmid per droplet. Each point represents one droplet. The line is the axis $x = y$. **d**, Uncorrelated, correlated and total noise 100 min after the start of fluorescence increase for a range of DNA concentrations. The dashed line represents the background noise due to imaging and analysis (Supplementary Fig. 6). **e**, Uncorrelated noise values for the DNA range at 10, 30, 50 and 100 min after the start of fluorescence increase. **f**, Uncorrelated noise values for the DNA range at different time points where the total protein concentration had reached 0.2 μM. In **b**,**d**–**f**, error bars show 95% confidence intervals, which were calculated by bootstrapping from the original distribution.

100 min after the start of fluorescence increase, as this yielded higher signal-to-background ratios and thus more reliable data. We also plotted uncorrelated noise at 0.2 μM of average protein production over the population of droplets for all DNA copy numbers (Fig. 2f and Supplementary Fig. 8) to confirm that the noise increases as we decrease the copy number.

Macromolecular crowding enhances uncorrelated noise

After exploring the range of copy numbers that can be studied reliably, we added Ficoll 70, a common macromolecular crowding agent, to mimic the crowded conditions inside cells[34,35]. Remarkably, the addition of 90 mg ml^{-1} Ficoll led to strikingly different production levels for CFP and YFP over the population of droplets (that is, the uncorrelated noise increased significantly) (Fig. 3a,b and Supplementary Fig. 9).

We performed cell-free gene expression in the presence of 40, 70 and 90 mg ml^{-1} Ficoll for a range of DNA concentrations and compared the uncorrelated noise values to results from experiments using 0 mg ml^{-1} Ficoll (Fig. 3c and Supplementary Fig. 10). Cell-free gene expression in the presence of 40 mg ml^{-1} Ficoll shows similar levels of uncorrelated noise as in the absence of Ficoll (Fig. 3d), yet the results for both 70 mg ml^{-1} (Fig. 3e) and 90 mg ml^{-1} (Fig. 3f) Ficoll show enhancement of uncorrelated noise. At ~600 copies of each plasmid, uncorrelated noise values are 0.11, 0.10, 0.19 and 0.21 for 0, 40, 70 and 90 mg ml^{-1} Ficoll, respectively.

The average protein expression rates (Supplementary Methods) in droplets following the addition of Ficoll are comparable to droplets without Ficoll (Fig. 4a and Supplementary Fig. 11), confirming that the increase in uncorrelated noise with increasing Ficoll concentrations is not due to lower protein production. Furthermore, the uncorrelated noise at the same protein concentration shows the same trend for all Ficoll concentrations (Supplementary Fig. 12). To understand how crowding leads to enhanced levels of uncorrelated noise in cell-free protein expression we probed the influence of the physical environment on molecular processes. We used fluorescent recovery after photo-bleaching (FRAP) to determine the diffusion coefficient of Alexa 647-labelled 70S ribosomes (Supplementary Fig. 13 and Supplementary Methods). As expected, the diffusion coefficients decrease as the Ficoll concentration is increased (Fig. 4b). We find a diffusion coefficient of 4.7 ± 0.215 μm^2 s^{-1} in the absence of Ficoll and 0.4 ± 0.001 μm^2 s^{-1} in the presence of 90 mg ml^{-1} Ficoll.

Noting these significantly lower diffusion constants for ribosomes in crowded solutions, we decided to study the spatial distribution of mRNA. Limited diffusion induced by macromolecular crowding could potentially hinder the homogeneous distribution of *in situ* synthesized mRNA molecules[21,36], thereby increasing the heterogeneity and consequently the uncorrelated noise. To investigate the distribution and localization of the mRNA in crowded and dilute solutions, we studied an *in vitro* transcription-only system using a DNA sequence encoding for a 32-repeat sequence (pET-32xBT) of a hybridization target for a molecular beacon (Supplementary Fig. 14 and Supplementary Methods). This method has previously been used successfully *in vivo*[37], and allows the visualization of mRNA production using confocal microscopy. *In vitro* transcription was performed in droplets in the absence of Ficoll and in the presence of 90 mg ml^{-1} Ficoll (Fig. 5a). Without Ficoll there is a homogeneous distribution of mRNA molecules and a gradual increase in fluorescence in the droplets, whereas droplets with the crowding agent show the appearance of spots over time, indicating local areas of high concentrations of mRNA. These spots disappear when transcription stops, indicating that they are not aggregates of mRNA. We followed the number of spots over time for two separate experiments (Fig. 5b and Supplementary Fig. 15), and in both cases observed an increase in the number of detectable spots for approximately the first 50 min, followed by a decrease. We note that the absolute number of spots detected is quite low; we can see many more very small spots, but

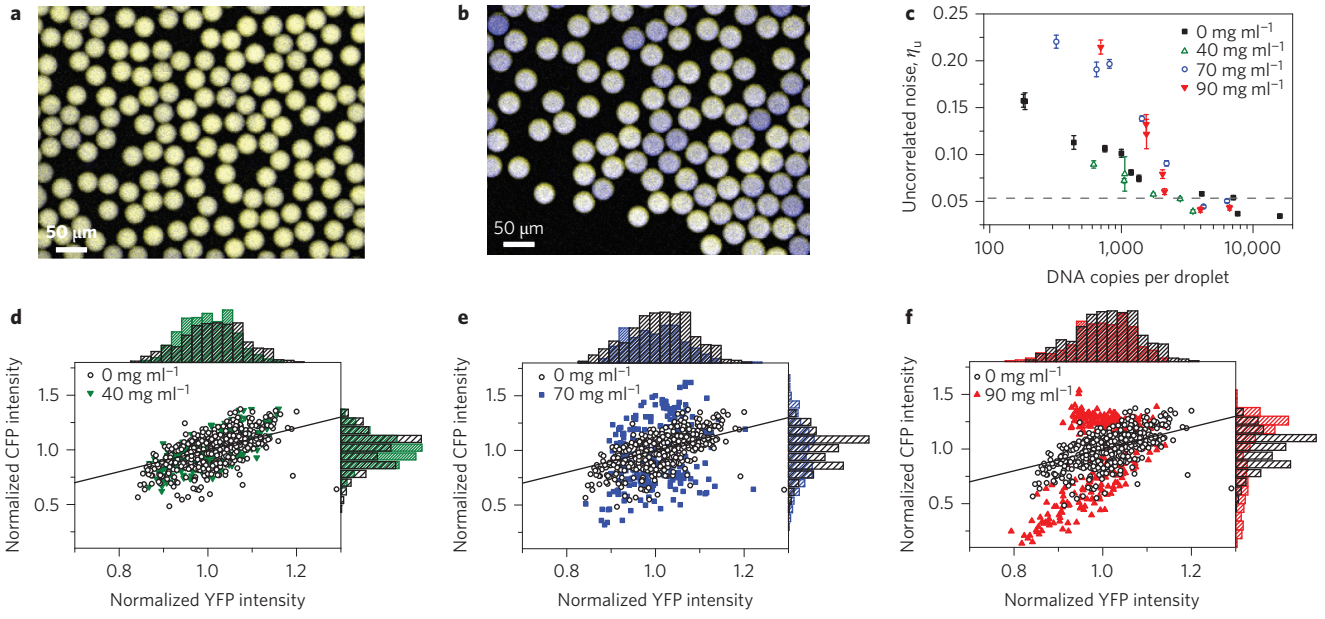

Figure 3 | Enhancement of uncorrelated noise in the presence of Ficoll. a, Superimposed false-colour images. CFP and YFP levels are similar in the dilute droplets, with ~600 copies of each plasmid per droplet. **b**, Super-imposed false-colour images. CFP and YFP levels show high variability over a population of droplets due to differences in CFP and YFP expression within the same droplet at 90 mg ml^{-1} Ficoll, with ~600 copies of each plasmid per droplet. **c**, Uncorrelated noise at 100 min after start of expression for a range of DNA concentrations at different Ficoll concentrations: 0, 40, 70 and 90 mg ml^{-1}. The dashed line represents the background noise due to imaging and analysis (Supplementary Fig. 6) and error bars show 95% confidence intervals, which were calculated by bootstrapping from the original distribution. **d**–**f**, Normalized CFP versus normalized YFP intensities of the whole population of droplets at 100 min after the start of expression: 0, 40, 70 and 90 mg ml^{-1} Ficoll, for ~600 copies of plasmid per droplet. Each point represents one droplet.

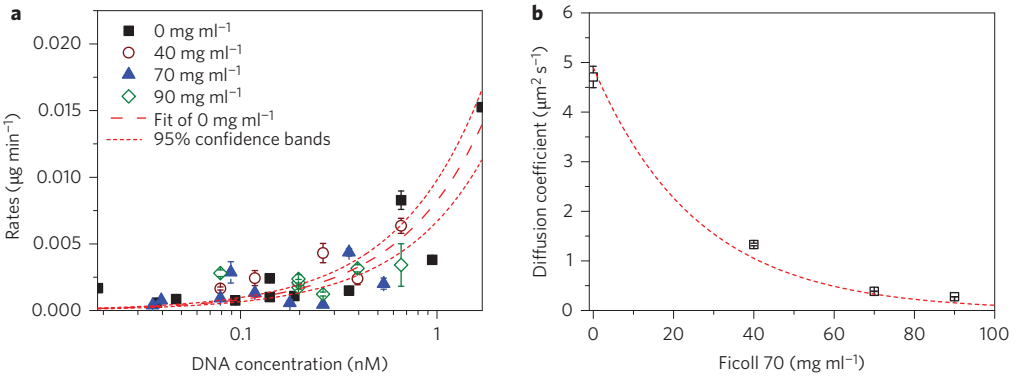

Figure 4 | Protein expression rates and ribosomal diffusion coefficients. a, CFP expression rates for 0, 40, 70 and 90 mg ml^{-1} with linear fit for 0 mg ml^{-1}, showing 95% confidence bands, error bars represent the error in fitting the protein expression curves. **b**, Diffusion coefficients of ribosomes over a range of Ficoll concentrations determined using fluorescence recovery after photobleaching experiments, error bars represent the error in fitting the recovery curves. The dashed line is a Stokes–Einstein fit of the diffusion coefficient $D \sim 1/\mu$, where μ is the concentration-dependent dynamic viscosity of Ficoll (Supplementary Methods).

they fall below our signal-to-noise threshold. The spots have a constant average fluorescence intensity over time (Fig. 5c), indicating that there is equilibrium between the production and dissipation of mRNA. However, the fluorescence intensity of the whole droplet increases for the first 50 min, which supports the argument that mRNA is constantly dissipating from its production point. As spots start disappearing after 50 min, the average intensity of the droplet reaches a plateau; the spots disappear because as the production of mRNA halts, only dissipation occurs. The number of spots scales linearly with DNA copy number (Supplementary Fig. 15). These results imply that the spots are local production sites of mRNA. The spots were absent when no DNA was added, and we verified that they did not result from aggregation of mRNA and a molecular beacon induced by Ficoll (Supplementary Fig. 16). In other words, transcription in crowded droplets leads to a heterogeneous distribution of mRNA molecules over the time course of mRNA expression, similar to the limited diffusion of mRNA molecules observed in *Escherichia coli* cells[21]. The formation of high local concentrations of mRNA can be explained by an imbalance in production rates and diffusion rates, the latter dropping significantly in crowded solutions (Fig. 4b). We note that the inhomogeneous production of proteins cannot be observed, as they will have distributed homogeneously over the droplet volume before their fluorophores matured.

Crowding causes microenvironment formation

To understand under what conditions the mRNA will be distributed heterogeneously in a coupled transcription translation reaction—in other words, at what point the local synthesis rate of mRNA exceeds the local diffusion rate of mRNA (Fig. 6a)—we calculated the time it

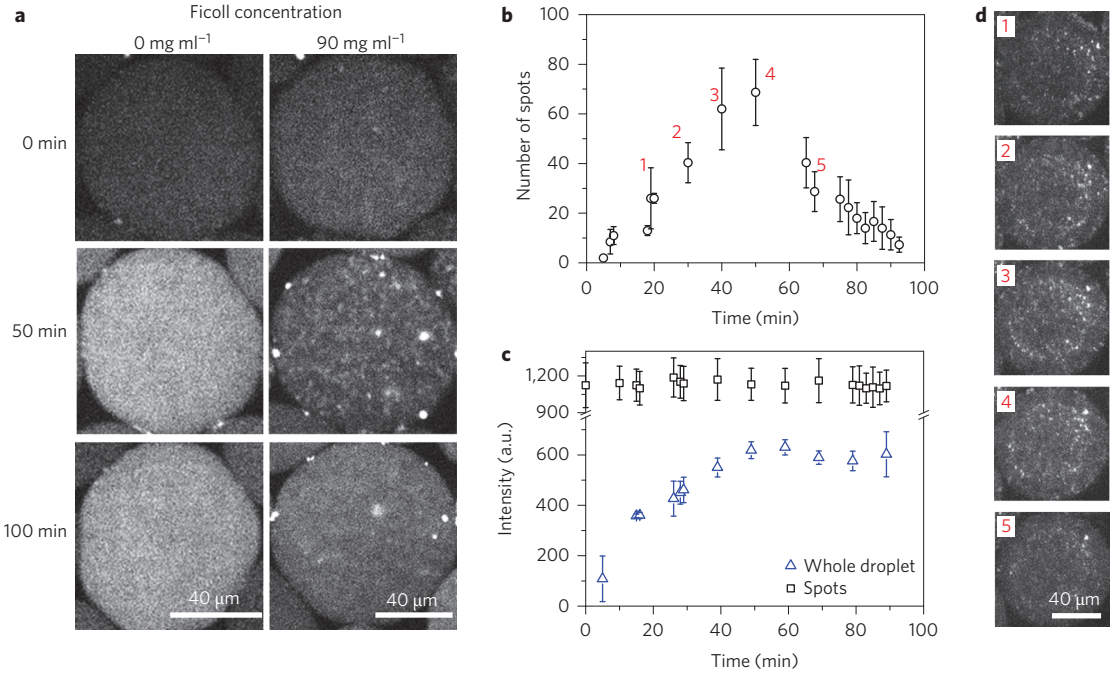

Figure 5 | Inhomogeneous distribution of mRNA over one droplet at high Ficoll concentrations. a, *In vitro* transcription-only experiments with 0.6 nM pET-32xBT showing mRNA expression with 0 mg ml^{-1} (left) and 90 mg ml^{-1} (right) Ficoll, in the presence of molecular beacon. **b**, Average number of spots over time from three separate droplets (circles) with error bars showing standard deviations. **c**, Average fluorescence intensity over time for the detected spots (squares) and whole droplets (triangles). Error bars are standard deviations of three separate droplets. **d**, Representative fluorescence images corresponding to the labelled time points in **b**.

would take for one mRNA to be produced (Fig. 6b, black line) using Michaelis–Menten kinetics with a typical K_m of 0.5 nM and V_{max} of 0.1 nM min^{-1} (derived experimentally, Supplementary Fig. 17). Newly produced mRNA becomes bound by ribosomes; multiple ribosomes interacting with one mRNA can associate into a polysome, and diffusion coefficients for these polysomal complexes were estimated using the Stokes–Einstein equation (Supplementary Fig. 18). We assume that the plasmids are distributed homogeneously (Supplementary Fig. 19) with an average distance $d \sim c^{-1/3}$. We thus calculated the average rate (in s^{-1}) for a polysome to diffuse over a distance $d/2$ (Fig. 6b, red line). We found that below 50 mg ml^{-1} Ficoll, the diffusion is typically higher than mRNA production, resulting in no localization, and above 50 mg ml^{-1} the opposite is the case, resulting in localization. Not much is known about the exact mechanism of localized transcription and translation in bacterial cells, although there has been much speculation that slower diffusion plays a role[21,38]. Our results indicate that the decreased diffusion caused by molecular crowding could indeed play a prominent role in localized gene expression.

To estimate the relative contribution of the different factors influencing uncorrelated noise, we simulated the stochastic cell-free gene expression in 200 droplets using Gillespie's Direct Method algorithm (Supplementary Methods and Fig. 6c). Again, we used the same K_m and V_{max} values for transcription previously established. For translation, a K_m value from Stögbauer and co-workers was used[39], and V_{max} was estimated from our experimental results. We measured protein maturation times (Supplementary Fig. 20) at different Ficoll concentrations and included these in the model. The uncorrelated noise versus plasmid copy number was plotted by taking the uncorrelated noise values after 100 min. The transcription and translation were first simulated with stochasticity as the only contributing factor, thereby excluding the Poisson distribution of plasmids, protein maturation and crowding. Later, the other factors were included in the model one by one to determine the contribution of each factor separately (Fig. 6d and Supplementary Fig. 21). The crowded droplets were simulated using a 10 times higher probability for a ribosome to rebind to the same mRNA (denoted p.n-1). An enhanced rebinding probability is supported by the observation and explanation of mRNA localization discussed above. The translationally active machinery must be co-localized with the mRNA, and this creates local microenvironments with higher concentrations of biologically active transcription and translation machinery, that is, the accumulation of ribosomes at plasmids. Owing to the lower diffusivity, this machinery has a higher probability of rebinding than anticipated from a homogeneous distribution of all components.

The results from the stochastic simulation show a decrease in uncorrelated noise with increasing copy number, which is consistent with our experimental data. Importantly, the model also shows that the trend of uncorrelated noise over plasmid copy number is not due to population differences in mean (CFP and YFP concentration) over the range of DNA copy numbers, which is also consistent with our experimental findings (Supplementary Figs 12 and 22). We find that the CFP and YFP maturation times have almost no effect on uncorrelated noise (mean of 1% over the plasmid copy numbers), while the average contributions over the plasmid copy numbers of stochasticity, Poisson distributions of plasmids and crowding are 18, 40 and 41%, respectively (Supplementary Fig. 20).

Conclusions

By studying gene expression in picolitre droplets, we can reliably analyse the uncorrelated and correlated noise of protein expression of low copy numbers of DNA under different physical conditions. Surprisingly, we find that an increase in macromolecular crowding, leading to an order-of-magnitude decrease in the diffusion coefficients of RNA and proteins, leads to significantly enhanced uncorrelated noise. At the same time, we observe that mRNA becomes distributed heterogeneously over the droplet, creating local microenvironments where gene expression occurs. Owing to the formation of large polysomes, biologically active machinery will be less likely to

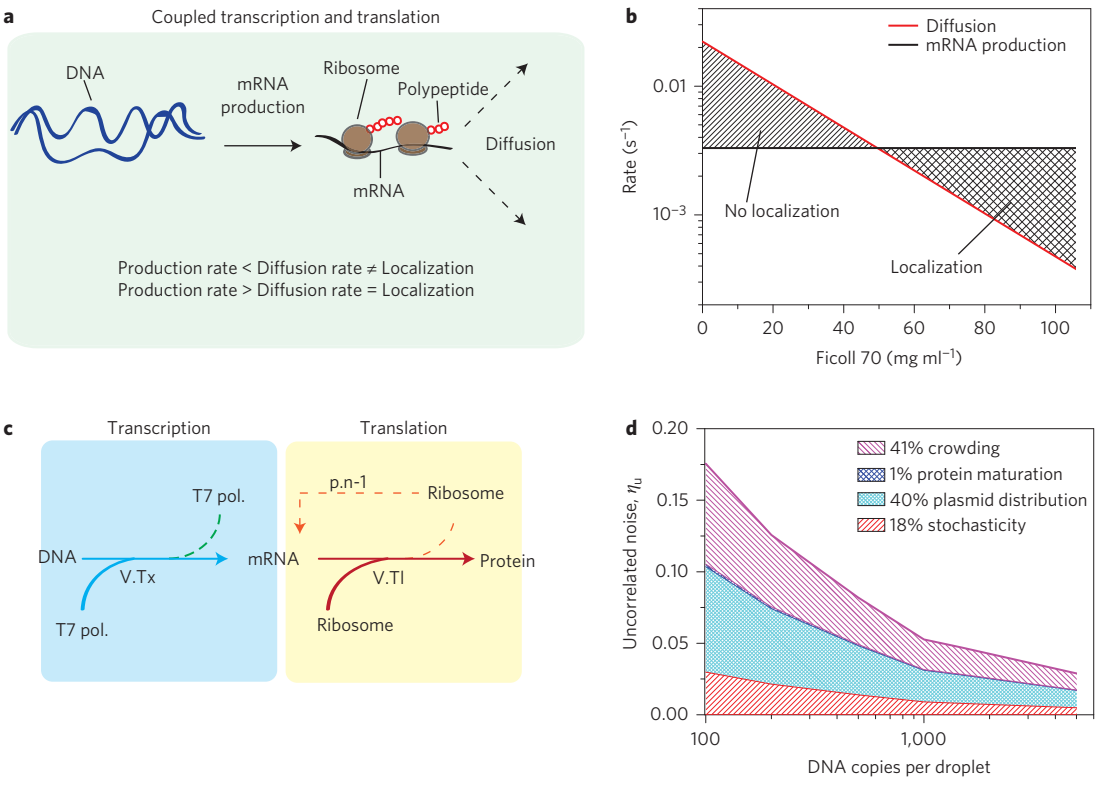

Figure 6 | Theoretical modelling of gene expression noise. a, During *in vitro* transcription and translation, all the biologically active machinery is unlikely to localize at the production site if the production rate is smaller than the diffusion rate, and is likely to localize at the production site if the production rate is larger than the diffusion rate. **b**, Theoretical model predictions of mRNA production (black line) and polysome diffusion over half the average distance between two plasmids (red line). The crossover between both rates indicates the transition between a homogeneous distribution of mRNA and an overall localization of mRNA, therefore showing the Ficoll concentrations at which we would see localization and which not. **c**, Schematic illustration of the stochastic transcription–translation model used in crowded droplets. Owing to the formation of microenvironments, ribosomes preferentially rebind to previous mRNA (denoted n-1). **d**, Simulation results showing the contributions of all factors to the total uncorrelated noise. Stochasticity is shown in red, plasmid distribution in light blue, protein maturation in dark blue, and crowding in violet.

diffuse away from these microenvironments. This lack of diffusion maintains the heterogeneous environment and enhances any already existing stochasticity caused by transcription and translation of low copies of DNA. Theoretical modelling strongly supports this theory, showing that the heterogeneous display of mRNA is caused by a fine balance between mRNA production rates and diffusion times. Furthermore, the results of the stochastic simulations suggest that any existing bias towards one of the two fluorescent proteins is strongly enhanced by preferential rebinding of ribosomes to the same mRNA, which we believe is the cause of our observed enhanced uncorrelated noise in crowded droplets.

These results are the first to show that the stochasticity of biochemical reactions is governed by the interplay between the rate of the reaction and its environment. Our experimental finding of heterogeneous mRNA distributions in crowded *in vitro* transcription systems and the concomitant increase in uncorrelated noise in similarly crowded cell-free expression systems has important implications for our understanding of living cells. It is very much conceivable that the synthesis of macromolecules (mRNA and proteins) *in vivo* leads to locally heterogeneous systems, as production rates will often be larger than diffusion rates[21]. This might explain the findings in the literature on the localization of mRNA in *E. coli*[21,38], but also helps to explain the origin of experimentally determined uncorrelated noise in gene expression[40]. Finally, our experiments enable us not only to take into account, but also predict the magnitude of stochasticity when designing synthetic chemical pathways similar to artificial cell-like systems.

Methods

Methods and any associated references are available in the online version of the paper.

Received 22 December 2014; accepted 15 September 2015; published online 26 October 2015

References

1. Maamar, H., Raj, A. & Dubnau, D. Noise in gene expression determines cell fate in *Bacillus subtilis*. *Science* **317,** 526–529 (2007).
2. Chang, H. H., Hemberg, M., Barahona, M., Ingber, D. E. & Huang, S. Transcriptome-wide noise controls lineage choice in mammalian progenitor cells. *Nature* **453,** 544–547 (2008).
3. Graf, T. & Stadtfeld, M. Heterogeneity of embryonic and adult stem cells. *Cell Stem Cell* **3,** 480–483 (2008).
4. Gupta, P. B. *et al.* Stochastic state transitions give rise to phenotypic equilibrium in populations of cancer cells. *Cell* **146,** 633–644 (2011).
5. Weinberger, L. S., Burnett, J. C., Toettcher, J. E., Arkin, A. P. & Schaffer, D. V. Stochastic gene expression in a lentiviral positive-feedback loop: HIV-1 Tat fluctuations drive phenotypic diversity. *Cell* **122,** 169–182 (2005).
6. Yu, J., Xiao, J., Ren, X., Lao, K. & Xie, X. S. Probing gene expression in live cells, one protein molecule at a time. *Science* **311,** 1600–1603 (2006).
7. Hensel, Z. *et al.* Stochastic expression dynamics of a transcription factor revealed by single-molecule noise analysis. *Nature Struct. Mol. Biol.* **19,** 797–802 (2012).
8. Munsky, B., Neuert, G. & van Oudenaarden, A. Using gene expression noise to understand gene regulation. *Science* **336,** 183–187 (2012).
9. Pedraza, J. M. & Paulsson, J. Effects of molecular memory and bursting on fluctuations in gene expression. *Science* **319,** 339–343 (2008).
10. Mettetal, J. T., Muzzey, D., Pedraza, J. M., Ozbudak, E. M. & van Oudenaarden, A. Predicting stochastic gene expression dynamics in single cells. *Proc. Natl Acad. Sci. USA* **103,** 7304–7309 (2006).
11. Elowitz, M. B., Levine, A. J., Siggia, E. D. & Swain, P. S. Stochastic gene expression in a single cell. *Science* **297,** 1183–1186 (2002).

12. Hilfinger, A. & Paulsson, J. Separating intrinsic from extrinsic fluctuations in dynamic biological systems. *Proc. Natl Acad. Sci. USA* **108,** 12167–12172 (2011).
13. Raser, J. M. & O'Shea, E. K. Control of stochasticity in eukaryotic gene expression. *Science* **304,** 1811–1814 (2004).
14. Nishimura, K., Tsuru, S., Suzuki, H. & Yomo, T. Stochasticity in gene expression in a cell-sized compartment. *ACS Synth. Biol.* **4,** 566–576 (2015).
15. Shahrezaei, V. & Swain, P. S. The stochastic nature of biochemical networks. *Curr. Opin. Biotechnol.* **19,** 369–374 (2008).
16. Weitz, M. *et al.* Diversity in the dynamical behaviour of a compartmentalized programmable biochemical oscillator. *Nature Chem.* **6,** 295–302 (2014).
17. Bratsun, D., Volfson, D., Tsimring, L. S. & Hasty, J. Delay-induced stochastic oscillations in gene regulation. *Proc. Natl Acad. Sci. USA* **102,** 14593–14598 (2005).
18. Elowitz, M. B. & Leibler, S. A synthetic oscillatory network of transcriptional regulators. *Nature* **403,** 335–338 (2000).
19. Zimmerman, S. B. & Harrison, B. Macromolecular crowding increases binding of DNA polymerase to DNA: an adaptive effect. *Proc. Natl Acad. Sci. USA* **84,** 1871–1875 (1987).
20. Minton, A. P. How can biochemical reactions within cells differ from those in test tubes? *J. Cell Sci.* **119,** 2863–2869 (2006).
21. Montero Llopis, P. *et al.* Spatial organization of the flow of genetic information in bacteria. *Nature* **466,** 77–81 (2010).
22. Klumpp, S., Scott, M., Pedersen, S. & Hwa, T. Molecular crowding limits translation and cell growth. *Proc. Natl Acad. Sci. USA* **110,** 16754–16759 (2013).
23. Brangwynne, C. P. *et al.* Germline P granules are liquid droplets that localize by controlled dissolution/condensation. *Science* **324,** 1729–1732 (2009).
24. Parry, B. R. *et al.* The bacterial cytoplasm has glass-like properties and is fluidized by metabolic activity. *Cell* **156,** 183–194 (2014).
25. Swain, P. S., Elowitz, M. B. & Siggia, E. D. Intrinsic and extrinsic contributions to stochasticity in gene expression. *Proc. Natl Acad. Sci. USA* **99,** 12795–12800 (2002).
26. Acar, M., Mettetal, J. T. & van Oudenaarden, A. Stochastic switching as a survival strategy in fluctuating environments. *Nature Genet.* **40,** 471–475 (2008).
27. van Zon, J. S., Morelli, M. J., Tănase-Nicola, S. & ten Wolde, P. R. Diffusion of transcription factors can drastically enhance the noise in gene expression. *Biophys. J.* **91,** 4350–4367 (2006).
28. Courtois, F. *et al.* An integrated device for monitoring time-dependent *in vitro* expression from single genes in picolitre droplets. *ChemBioChem* **9,** 439–446 (2008).
29. Karig, D. K., Jung, S.-Y., Srijanto, B., Collier, C. P. & Simpson, M. L. Probing cell-free gene expression noise in femtoliter volumes. *ACS Synth. Biol.* **2,** 497–505 (2013).
30. Sokolova, E. *et al.* Enhanced transcription rates in membrane-free protocells formed by coacervation of cell lysate. *Proc. Natl Acad. Sci. USA* **110,** 11692–11697 (2013).
31. Shim, J.-u. *et al.* Simultaneous determination of gene expression and enzymatic activity in individual bacterial cells in microdroplet compartments. *J. Am. Chem. Soc.* **131,** 15251–15256 (2009).
32. Paulsson, J. Summing up the noise in gene networks. *Nature* **427,** 415–418 (2004).
33. Dunlop, M. J., Cox, R. S., Levine, J. H., Murray, R. M. & Elowitz, M. B. Regulatory activity revealed by dynamic correlations in gene expression noise. *Nature Genet.* **40,** 1493–1498 (2008).
34. Ellis, R. J. Macromolecular crowding: obvious but underappreciated. *Trends Biochem. Sci.* **26,** 597–604 (2001).
35. Ge, X., Luo, D. & Xu, J. Cell-free protein expression under macromolecular crowding conditions. *PLoS ONE* **6,** e28707 (2011).
36. Gillespie, D. T., Petzold, L. R. & Seitaridou, E. Validity conditions for stochastic chemical kinetics in diffusion-limited systems. *J. Chem. Phys.* **140,** 054111 (2014).
37. Vargas, D. Y., Raj, A., Marras, S. A. E., Kramer, F. R. & Tyagi, S. Mechanism of mRNA transport in the nucleus. *Proc. Natl Acad. Sci. USA* **102,** 17008–17013 (2005).
38. Kim, S., Mlodzianoski, M., Bewersdorf, J. & Jacobs-Wagner, C. Probing spatial organization of mRNA in bacterial cells using 3D super-resolution microscopy. *Biophys. J.* **102,** 278a (2012).
39. Stogbauer, T., Windhager, L., Zimmer, R. & Radler, J. O. Experiment and mathematical modeling of gene expression dynamics in a cell-free system. *Integr. Biol.* **4,** 494–501 (2012).
40. Ozbudak, E. M., Thattai, M., Kurtser, I., Grossman, A. D. & van Oudenaarden, A. Regulation of noise in the expression of a single gene. *Nature Genet.* **31,** 69–73 (2002).

Acknowledgements

The authors thank R.Y. Tsien for kindly donating the genes encoding for YFP and CFP, F.H.T. Nelissen and D. Foschepoth for assisting with cloning work, E. Dubuc for designing the molecular beacon, and J. Thiele for designing the masters for the fluidic devices. This work was supported by a European Research Council (ERC) Advanced Grant (246812 Intercom), a VICI grant from the Netherlands Organization for Scientific Research (NWO), and funding from the Ministry of Education, Culture and Science (Gravity programme, 024.001.035).

Author contributions

M.H., L.M. and W.H. conceived and designed the experiments. M.H., L.M., R.M. and M.V.R. performed the experiments. M.H. and L.M. analysed the data. E.S., J.G. and H.H. contributed materials/analysis tools. M.H. and W.H. co-wrote the paper.

Additional information

Supplementary information is available in the online version of the paper. Reprints and permissions information is available online at www.nature.com/reprints. Correspondence and requests for materials should be addressed to W.T.S.H.

Competing financial interests

The authors declare no competing financial interests.

Methods

Device fabrication. The design of the microfluidic devices was produced using AutoCAD. The wafers contain a negative relief in SU-8 photoresist on a silicon wafer substrate. The channels for the droplet production are 25 μm in width. To make the microfluidic devices, crosslinker and polydimethylsiloxane (PDMS) were added together in a ratio of 1:10 and the solution was poured on the wafers (cleaned with isopropanol). Air bubbles were removed using a desiccator. Thereafter, the devices were put in the oven at 65 °C for at least 2 h. After preparing the PDMS layer, the device was bonded on a glass slide by activating the PDMS and glass surfaces using plasma cleaner (Femto), after which the surfaces were bonded together. Air between the surfaces was removed by applying pressure gently. The device was incubated for at least 3 h at 100 °C, after which the device was coated with a 2% silane solution.

Device and set-up operation. Liquids were pumped into microfluidic devices using adjustable pumps (Harvard apparatus, PHD 2000 infusion) connected to a syringe via polytetrafluoroethylene tubing (inner diameter of 0.056 mm; outer diameter of 1.07 mm). Droplets in the microfluidics were stabilized using a 2% biocompatible Krytox-based tri-block copolymer surfactant in Fluorinert FC-40 oil (Sigma-Aldrich) or hydrofluoroether (HFE).

Data acquisition and analysis. The devices were mounted on an inverted microscope (Olympus IX81) equipped with a motorized stage (Prior, Optiscan II). Fluorescence images were taken with a sensitive-electron multiplying charge-coupled device camera (iXon, Andor) using illumination from a mercury lamp. Analysis of the images was performed using a home-written Matlab routine.

Plasmids. pET plasmids with CFP and YFP sequences at multiple clone sites were a gift from R.Y. Tsien. The sequences for CFP and YFP production in the pET plasmids were inserted into pRSET vectors (Life Technologies) with Nco-I at the 5′ end of the coding sequence (CDS) and a Xho-I restriction site at the 3′ end. The plasmids were purified, and the purity was analysed using gel electrophoresis and sequencing analysis (GATC Biotech). The concentration of plasmids was determined using a Nanodrop N1000 spectrophotometer. The pRSET vector had T7 RNAP promoter and terminator regions.

Lysate preparation. *E. coli* Rosetta2 cells were grown at 37 °C to $OD_{600} = 1.5$ in 2YTPG broth. After cell growth, all subsequent steps were conducted over ice. The cells were collected (3,000*g*, 10 min, 4 °C), thoroughly dissolved in ice-cold 20% sucrose solution (16 ml for 3 g wet pellet weight) and incubated on ice for 10 min. Cells were then collected (3,000*g*, 10 min, 4 °C), resuspended in ice-cold milli-Q (MQ) (4 × wet pellet weight) and immediately spun down (3,000*g*, 10 min, 4 °C). Cells were resuspended in ice-cold MQ (4 × wet pellet weight), allowed to incubate on ice for 10 min and spun down (3,000*g*, 10 min, 4 °C). The pellet was then carefully washed twice with ice-cold MQ (1.5 × volume). The spheroplast pellet was stored at −80 °C.

The spheroplasts were thawed and resuspended in ice-cold MQ (0.8 × volume). Cells were lysed with 10 cycles of sonication (10 s at 10 μm amplitude followed by 30 s on ice). Cell debris was collected (30,000*g*, 30 min, 4 °C) and dialysed ×1 against 50% dialysis buffer (5 mM Tris, 30 mM potassium glutamate, 7 mM magnesium glutamate, 0.5 mM dithiothreitol, DTT) and 3 × 100% dialysis buffer (10 mM Tris, 60 mM potassium glutamate, 14 mM magnesium glutamate, 1 mM DTT).

***In vitro* transcription/translation mixture.** For transcription–translation systems, the reaction mixtures consisted of one-third cell lysate from BL21 (DE3) host strain (~25 mg ml^{-1}) and two-thirds reaction buffer. The final reaction mixture contained 50 mM Hepes (pH 8.0), 2.4 mM guanosine triphosphate, 1 mM each of adenosine triphosphate, cytidine triphosphate and uridine triphosphate, 0.66 mM spermidine, 0.5 mM cyclic adenosine monophosphate, 0.22 mM nicotinamide adenine dinucleotide, 0.17 mM coenzyme A, 20 mM 3-phosphoglyceric acid, 0.045 mM folinic acid, 0.13 mg ml^{-1} transfer ribonucleic acid, 1 mM of each amino acid, 10 mM magnesium glutamate, 66 mM potassium glutamate, 130 U T7 RNA polymerase and 8.3 mg ml^{-1} cell lysate, contributing an additional 5 mM magnesium glutamate and 20 mM potassium glutamate. Plasmids were added last to initialize transcription.